RESEARCH ARTICLE

Phytoplankton community structuring in the absence of resource-based competitive exclusion

Michael J. Behrenfeld[1]*, **Kelsey M. Bisson**[1], **Emmanuel Boss**[2], **Peter Gaube**[3], **Lee Karp-Boss**[2]

1 Department of Botany and Plant Pathology, Oregon State University, Corvallis, OR, United States of America, **2** School of Marine Sciences, University of Maine, Orono, ME, United States of America, **3** Applied Physics Laboratory, University of Washington, Seattle, Washington, United States of America

☯ These authors contributed equally to this work.
* mjb@science.oregonstate.edu

Abstract

Under most natural marine conditions, phytoplankton cells suspended in the water column are too distantly spaced for direct competition for resources (i.e., overlapping cell boundary layers) to be a routine occurrence. Accordingly, resource-based competitive exclusion should be rare. In contrast, contemporary ecosystem models typically predict an exclusion of larger phytoplankton size classes under low-nutrient conditions, an outcome interpreted as reflecting the competitive advantage of small cells having much higher nutrient 'affinities' than larger cells. Here, we develop mechanistically-focused expressions for steady-state, nutrient-limited phytoplankton growth that are consistent with the discrete, distantly-spaced cells of natural populations. These expressions, when encompassed in a phytoplankton-zooplankton model, yield sustained diversity across all size classes over the full range in nutrient concentrations observed in the ocean. In other words, our model does not exhibit resource-based competitive exclusion between size classes previously associated with size-dependent differences in nutrient 'affinities'.

Introduction

Our interpretation of observed ecological properties derives from our conceptions of the environment experienced by organisms and their interactions with other individuals. These conceptions are inevitably influenced by our own experiences, such that fundamental ecological concepts originally formulated from observations of macro-organisms (birds, mammals, trees, etc.) are often carried forward to very different systems (e.g., microbial communities). For example, principles of resource-based competitive exclusion first deduced from terrestrial communities [1] are commonly assumed equally valid for the phytoplankton [2]. At the other end of the spectrum, principles of physical-chemistry can be used to formulate expressions for biochemical reactions, such as the Michaelis-Menten equation for enzymatic reaction kinetics [3]. The mathematical curve that the Michaelis-Menten equation represents often provides an

excellent fit to observational data for far more complex systems (e.g., nutrient uptake in phytoplankton cells), but such results do not imply that associated equation variables carry a similar physiological meaning as those for single enzyme reactions.

The conceptions we have regarding the plankton world are formalized and tested in ecosystem models. For oligotrophic ocean regions, these models often predict the proliferation of small phytoplankton species at the expense (i.e., exclusion) of larger species [e.g., 4–7]. This outcome is interpreted as the consequence of resource-based competitive exclusion, where smaller cells have a greater 'affinity' for nutrients and thus can draw nutrients down to a level that will not sustain larger cells. These predictions of size-dependent exclusions are inconsistent with observations. In the oligotrophic ocean, small species may be both numerically- and biomass-dominant, but the phytoplankton size distribution is nevertheless a continuum, where large cells persist at lower abundances [e.g., 8, 9]. This fundamental inconsistency, which has been noted previously [e.g., 10], motivated the current exploration of how we might better conceive of, and subsequently model, the growth environment experienced by phytoplankton and their interactions with other individuals.

In the narrative below, we begin with a depiction of aquatic ecosystems where individual phytoplankton are distantly spaced across nearly the full range of naturally-occurring cell abundances. In such seascapes, resource-based competitive exclusion is unlikely, which is at odds with the above noted loss of species diversity in plankton ecosystem models under low-nutrient conditions. This contradiction suggests that there is something fundamentally incorrect about the models. One possibility is that the problem lies with the model treatment of phytoplankton taxonomic groups simply as integrated nutrient (e.g., nitrogen) stocks sharing (i.e., competing for) common nutrient resources, rather than from the perspective of how individual cells experience their growth environment. To explore this possibility, we develop a diffusion-based model framework that is consistent with the growth of distantly-spaced, non-competing individuals and which derives from the mechanistic underpinnings of production-resource relationships observed in laboratory populations under light-limiting and nutrient-limiting conditions. A problem that arises from this approach is that the underlying physics yield an untenable initial prediction of extreme size-dependent differences in phytoplankton division rates. However, this issue is resolved when the model is applied to nutrient conditions reflective of natural oceanographic settings. Interestingly, our diffusion-based expression can be equated to a Michaelis-Menten functional form, implying that the apparent problem with ecosystem models does not lie in the treatment of phytoplankton as fluid variables (i.e., uniformly distributed stocks of a chosen element). Given this finding, we modify a published multi-species model to demonstrate how a simple revision to the model equations allows all modeled phytoplankton size classes to be sustained across the full nutrient domain of ultra-oligotrophic to eutrophic conditions. As you will discover at the end of this narrative, the common loss of species diversity in contemporary ecosystem models under low nutrient conditions has nothing to do with resource-based competitive exclusion.

Cell spacing and resource competition

Edward Hulburt, using data collected during a series of field campaigns spanning from the north Atlantic gyre to highly productive coastal waters, quantified the average spacing between nutrient depletion zones (i.e., 'boundary layers') associated with neighboring phytoplankton cells [11]. His analysis indicated that cell concentrations (of microphytoplankton and large nanophytoplankton) greater than $\sim 10^8$ L^{-1} would be required for cell boundary layers to predominantly overlap and, thus, for direct resource competition to ensue. This requirement exceeded observed cell concentrations by at least two orders of magnitude across all sampled

environments, save two shallow coastal estuaries. Accordingly, he concluded that this spatial separation implies that "*no cell can affect any other, that no species can interact with another, through competition for nutrients*" in most natural environments and that this lack of resource-based competition is the explanation for Evelyn Hutchinson's [2] 'Paradox of the Plankton'.

In 1998, David Siegel [12] greatly expanded upon Hulburt's earlier work, quantitatively evaluating the discreteness of phytoplankton across the cellular size domain. He introduced two distribution variables (*DV*) to assess the likelihood of overlapping 'spheres of influence' (i.e., boundary layers). In the spatial domain, DV_λ was defined as the ratio of the diameter of a phytoplankton's sphere of influence (d_{soi}) to the average distance between adjacent cells (λ):

$$DV_\lambda \equiv \frac{d_{soi}}{\lambda}, \tag{1A}$$

where $DV_\lambda > 1$ indicates overlapping boundary layers and competition for resources, whereas $DV_\lambda < 1$ indicates that cells are too far apart to feel the effects of their neighbors (see Table 1

Table 1. Symbols/abbreviations, definitions, and units (in order of appearance in manuscript).

Symbol/ abbrev.	Definition	Units
λ	average distance between individual cells	μm
d_{soi}	diameter of cell boundary layer	μm
τ_λ	interaction time scale between cells	s
τ_{bio}	characteristic biological time scale	s
n	number of cells per unit water volume	cells m^{-3}
d	cell diameter	μm
d_0	reference diameter	μm
N_0	particle differential number concentration at d_0	ml μm^{-1}
$>$	absolute value of the size distribution slope	unitless
Vol	cell volume	μm^3
C	phytoplankton cellular carbon content	pg cell^{-1}
C_{phyto}	carbon mass of phytoplankton population	ng C ml^{-1}
Chl	chlorophyll mass of phytoplankton population	ng Chl ml^{-1}
Vol_{phyto}	total cell volume per unit water volume	ml ml^{-1}
S_∞	far-field nutrient concentration	mmol m^{-3} or mM
P	phytoplankton biomass in nutrient units	mmol m^{-3}
V_m^*	maximum specific nutrient uptake rate	d^{-1}
K_m	Michaelis-Menten half-saturation substrate concentration	mmol m^{-3}
m	non-grazing specific death rate of phytoplankton	d^{-1}
I_g	Light level to which phytoplankton are acclimated	mol quanta m^{-2} d^{-1}
P	carbon–specific photosynthetic rate	d^{-1}
P_{max}	carbon–specific light-saturated photosynthetic rate	d^{-1}
μ_m	maximum specific rate of cell division	d^{-1}
α_P	light-limited slope of *P-I* relationship	m^2 (mol quanta)$^{-1}$
I_K^p	light-saturation index of *P-I* curve	mol quanta m^{-2} d^{-1}
μ	specific rate of cell division	d^{-1}
α_μ	light-limited slope of division rate-irradiance (μ-I_g) relationship	μmol C m^2 (μmol quanta)$^{-1}$
I_r	light level where primary production equals the maintenance respiration rate	d^{-1}
I_K^μ	light-saturation index of μ-I_g relationship	μmol quanta m^{-2} d^{-1}
ν	nutrient uptake rate	mmol cell^{-1} d^{-1}

(*Continued*)

Table 1. (Continued)

| Symbol/ abbrev.	Definition	Units
V_m	maximum nutrient uptake rate	mmol cell^{-1} d^{-1}
α_v	initial slope of the relationship between v and S_∞	dm^3 d^{-1}
Q	cellular requirement for limiting nutrient	mmol cell^{-1}
K_m^{cell}	nutrient concentration where $v = 0.5\,V_m$ for cells acclimated to different S_∞	mM
S_0	concentration of given nutrient at the cell surface	mmol m^{-3} or mM
F_D	diffusional flux of nutrient to a stationary spherical cell	mmol μm^3 s^{-1} or fg μm^3 s^{-1}
D	diffusion coefficient	μm^2 s^{-1}
F'_D	cell volume-specific diffusional flux of nutrient to a stationary spherical cell	mmol μm s^{-1} or fg μm s^{-1}
υ	characteristic cell sinking or swimming velocity	μm s^{-1}
P_e	Péclet number	unitless
Sh	Sherwood number	unitless
A_F	Potential nutrient flux available for assimilation assuming 90% capture efficiency and accounting for cell movement	mmol μm s^{-1} or fg μm s^{-1}
$\mathbf{P}_i^N$	total nitrogen inventory of the ith phytoplankton size class	mmol m^{-3}
Z_i^N	total nitrogen inventory of the ith zooplankton size class	mmol m^{-3}
f_i	feeding size range of grazers and carnivores with respect to mean prey size	unitless
g_1	zooplankton grazing rate	m^3 mmol^{-1} d^{-1}
g_2	zooplankton ingestion efficiency	unitless
g_3	zooplankton linear mortality rate	d^{-1}
g_4	zooplankton density-dependent mortality rate	m^3 mmol^{-1} d^{-1}
κ	media outflow rate in the Ward et al. [10] chemostat model	d^{-1}

for summary of symbols and abbreviations). The second distribution variable (DV_τ) was introduced to account for interactions between cells over time:

$$DV_\tau \equiv \frac{\tau_{bio}}{\tau_\lambda}, \tag{1B}$$

where τ_{bio} is a characteristic biological time scale (e.g., time between cell divisions) and τ_λ is the time scale that a given phytoplankter will feel the effects of its neighbors. In the case of nutrient competition, DV_τ can be thought of as "*the rate at which neighboring cells are intercepting a given cell's potential nutrient supply in relation to the cell's intrinsic nutrient demand over its division cycle*" [12]. Here again, $DV_\tau > 1$ indicates that neighboring cells will influence a given phytoplankter's nutrient supply, while $DV_\tau < 1$ implies minimal competition for nutrients between cells.

To illustrate the relationship between cell size, abundance, and the potential for resource competition, Siegel [12] assumed spherical cells in a quiescent medium, that a given phytoplankton population is composed entirely of a single cell size, that a cell's boundary layer is five times larger than the cell's diameter, and that $\tau_{bio} = 1$ day [see Siegel [12] for details and discussion on sensitivity of results to these assumptions]. For these assumptions, the threshold cell abundances for direct resource competition can be found [i.e., solving Eqs 11 and 13 in Siegel [12] for $DV_\lambda = 1$ and $DV_\tau = 1$] and expressed as a function of cell diameter (Fig 1A). The salient results here are that threshold abundances increase rapidly with decreasing cell size (note the logarithmic scaling of the y-axis in Fig 1A) and that across the cell size domain of phytoplankton these thresholds greatly exceed typical cell concentrations found in natural ocean waters.
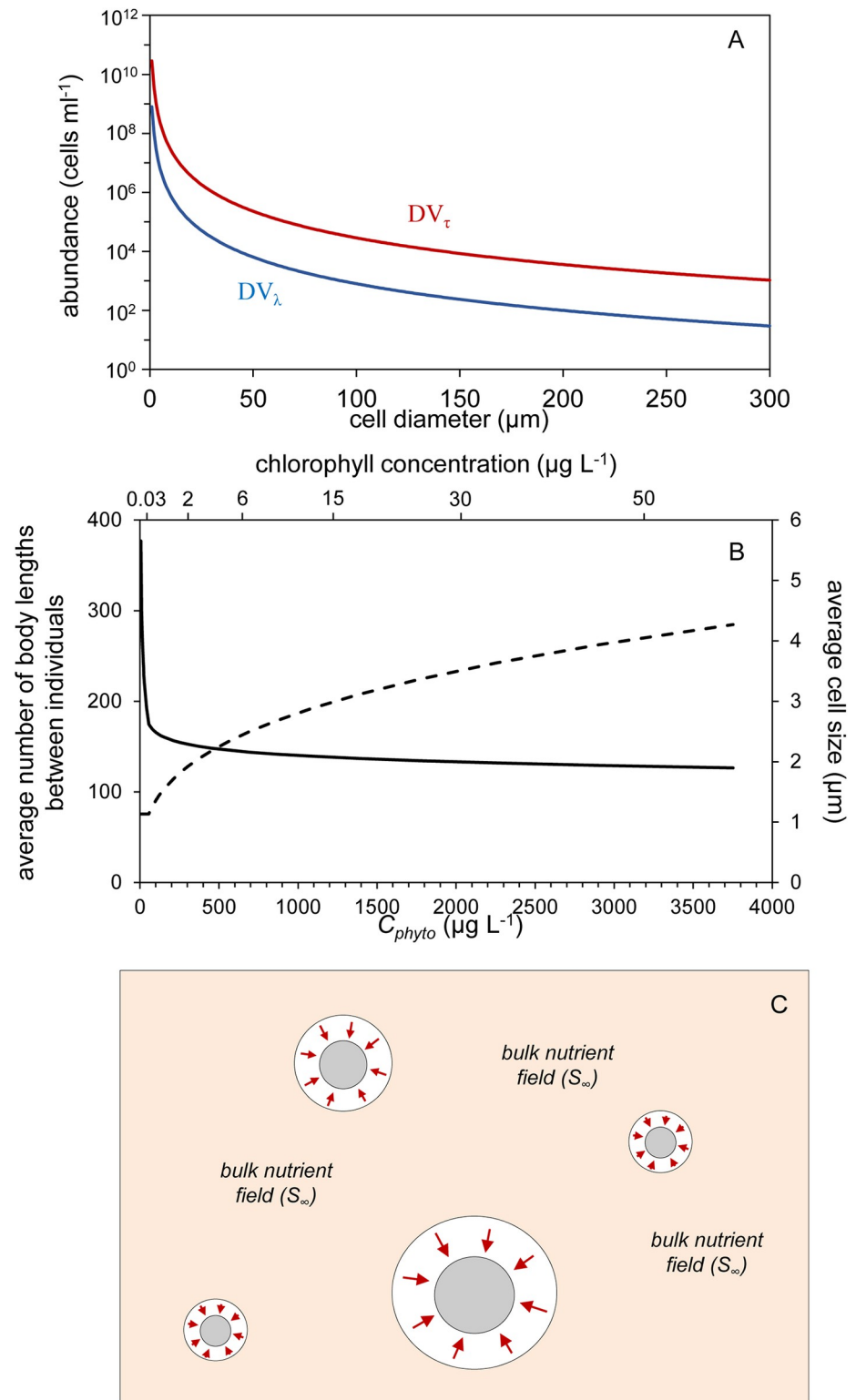
Fig 1. Conceiving the discreteness of phytoplankton communities. (A) Cell abundances for populations of a single cell size required for the spatial (DV_λ) and temporal (DV_τ) distribution variables defined by Siegel [12] to have a value of one, indicating direct competition for resources is prevalent. Note, these threshold values are notably larger than most natural population abundances. (B) Average number of body lengths between individual phytoplankton cells (left axis, solid line) and average population cell size (right axis, dashed line) for modeled phytoplankton communities with

size distributions reflective of natural populations (see text). Cell size is calculated as the cell diameter of the average cell volume. Bottom and top axis give total phytoplankton carbon biomass (C_{phyto}) and approximate corresponding chlorophyll concentrations. (C) Depiction of phytoplankton in natural waters where cells are distantly spaced and resource acquisition is limited to discrete boundary layers around each cell (outer circles with inward pointing arrows) and has no immediate impact on the far-field resource pool (S_∞) experienced by all cells.

We can further develop our conception, or 'intuition', regarding resource competition among phytoplankton by considering populations of a continuous size distribution. In stable lower-latitude oligotrophic systems, phytoplankton abundance is dominated by *Prochlorococcus*, with numbers typically ranging between 2 H 10^4 and 2 H 10^5 cells ml^{-1} [13, 14] and the phytoplankton community generally exhibits a size distribution with a slope of approximately -4.5 between the logarithm of cell number concentration per unit length and the logarithm of cell diameter (*d*) [15–19]. As nutrient stocks in the environment increase, *Prochlorococcus* abundances peak while the abundance of larger cells continues to increase, causing the size distribution slope to tilt upward toward -3 [19].

For the power-law size spectrum of phytoplankton communities [see Note 1 in S1 File], the total number of individuals [n (cells ml^{-1})] between two limits in size [d_{min}, d_{max} (μm)] can be calculated as:

$$n = \frac{d_0 N_0}{1 - \xi} \left\{ \left(\frac{d_{max}}{d_0} \right)^{1-\xi} - \left(\frac{d_{min}}{d_0} \right)^{1-\xi} \right\} \tag{2}$$

where $>$ is the absolute value of the size distribution slope, d_0 is a reference cell diameter (μm), and N_0 is the particle differential number concentration (ml μm^{-1}) at d_0. To demonstrate separation distances between phytoplankton cells in nature, we assign $d_0 = 1$ μm [see Note 2 in S1 File] and assume that $> = 4.5$ as available resources allow *Prochlorococcus* abundances to increase from 2 H 10^4 to 2 H 10^5 cells ml^{-1}. We further assume that additional increases in nutrients do not affect *Prochlorococcus* concentrations (i.e., remain capped at 2 H 10^5 cells ml^{-1}) but rather result in an increased abundance in larger cells such that $>$ decreases from 4.5 to 3.3. With these assumptions, the resultant total number of phytoplankton cells between d_{min} = 0.6 μm and d_{max} = 500 μm ranges from 3.2 H 10^4 to 4.1 H 10^5 cells ml^{-1} and the average cell size of the population increases from 1.1 to 4.3 μm as $>$ decreases from 4.5 to 3.3 (Fig 1B, dashed line, right axis). Assuming spherical cells and a non-diatom cellular carbon (*C*, pg cell^{-1}) to volume (*Vol*, μm^3) relationship of $C = 10^{-0.665+0.939 Log_{10}(Vol)}$ [20], the above defined phytoplankton populations span a biomass (C_{phyto}) range of 6 to ~3700 ng ml^{-1} (lower axis in Fig 1B; noting here that ng ml^{-1} = μg L^{-1}), or a chlorophyll (*Chl*) range of approximately 0.03 to 60 ng ml^{-1} assuming an increase in $Chl:C_{phyto}$ from 0.006 to 0.02 as biomass increases (due to self-shading). Thus, the modeled phytoplankton populations span a range from highly oligotrophic to highly eutrophic conditions, yet across this full range neighboring cells remain separated on average by 380 to 130 body lengths (Fig 1B, solid line, left axis).

As a final illustration of the diluteness of phytoplankton in nature, we can calculate the total cell volume per milliter of water (Vol_{phyto}) as:

$$Vol_{phyto} = \frac{1}{4->} \frac{\pi}{6} N_0 d_0^4 \left(\left(\frac{d_{max}}{d_0} \right)^{4-\xi} - \left(\frac{d_{min}}{d_0} \right)^{4-\xi} \right), \tag{3}$$

which, for a size range of 0.6–500 μm diameter, yields the result that phytoplankton only occupy 0.0000024% to 0.0017% of the volume in which they are suspended for the oligotrophic to eutrophic conditions considered above.

The foregoing analyses provide a general 'feel' for the distantly-spaced growth conditions experienced by phytoplankton in a steady-state environment, which is depicted schematically in Fig 1C ('schematically' because in nature cells are much further apart than illustrated). Of course, this schematic is incomplete and fails to recognize interactions that result from relative movements among cells due, for example, to active swimming, differences in sinking rates, small-scale turbulence, formation of thin layers of enhanced biomass, and other processes that bring cells into close proximity (even colliding and forming aggregates). These interactions can result in fleeting overlaps between cell boundary layers [quantified in 12 by the DV_τ variable] and, thus, direct competition for resources. In addition, the abundance of different phytoplankton groups also influences the far-field nutrient concentration (S_∞) experienced by all individuals (much like a change in abundance influences the light field experienced by all cells). For example, during the non-steady-state condition of a phytoplankton bloom, accumulation of a blooming species reduces the value of S_∞ experienced by all species (because resource is being drawn from the environment and sequestered into biomass). Likewise, in a nutrient-limited steady-state system, the biomass of different size classes is determined by predator-prey relationships that scale (not necessarily in a 1-to-1 fashion) with division rate. We will return to this latter idea below, but for the moment the central message conveyed in Fig 1 and above is that, to first order, phytoplankton experience their world as discrete entities with boundary layers rarely (on a day-to-day basis) overlapping with those of other individuals.

Given the above conception, the question arises whether discreteness of the phytoplankton requires a modification in how we model aquatic ecosystems? Essentially this same question was asked by David Siegel [12], who was considering the model construct:

$$\frac{d\mathbf{P}}{dt} = \sum_{i=1}^{i=j} \left(\frac{V_m^{*i} S_\infty}{S_\infty + K_m^i} \mathbf{P}_i - m\mathbf{P}_i \right), \tag{4}$$

where V_m^{*i} is the maximum specific uptake rate and K_m^i is substrate concentration at $^1/_2 V_m^{*i}$ for the ith phytoplankton group ($\mathbf{P}_i$) and m is the specific loss rate. In this formulation where growth rate is described in a Michaelis-Menten fashion, the phytoplankton community is simply expressed as the integrated stock of some nutrient element without explicit representation of individuals, thus it was concluded that:

"*Discreteness in phytoplankton. . .means that formulations of phytoplankton growth and interaction based upon assuming that planktonic organisms are fluid variables* [as in Eq 4 above] *are inappropriate for modeling phytoplankton population variations in natural waters. These models assume a priori that phytoplankton populations are distributed continuously, where every cell will uniformly and instantaneously feel the effects of its neighbor.*" [12]

The current authors have also voiced a similar concern [19, 21]. But, does the omission of discreteness in Eq 4 actually imply 'uniform and instantaneous' interactions that lead to competitive exclusion? We suggest below that, in fact, it does not. We build toward this conclusion by considering in the next section fundamental properties of phytoplankton production-resource relationships common to both light-limited and nutrient-limited growth.

Production-resource relationships

The relationship between phytoplankton production (e.g., photosynthesis, cell division) and resource supply can be described by equations requiring only two parameters. For the familiar Michaelis-Menten-type expression (e.g., Eq 4), these parameters are V_m and K_m when

describing nutrient-limited growth, with the latter term representing the fore-noted 'affinity' for a given resource. This interpretation of K_m has been promoted by laboratory competition experiments where species with lower K_m (i.e., greater affinity) ultimately displace (i.e., competitive exclusion) those with higher K_m [e.g., 22]. However, employing Michaelis-Menten-type expressions in ecosystem models raises a couple important issues. First, the Michaelis-Menten equation [3] was developed to describe single substrate-enzyme-product systems and is mechanistically grounded in physical-chemistry. When applied to whole-cell properties (beyond simply the behavior of membrane transporters), this mechanistic basis for the equation (thus, interpretation of model variables) is compromised. Second, it is not immediately clear whether expressions, such as Eq 4, provide robust predictions for populations of distantly-spaced phytoplankton cells, as noted in the previous section. In the following, we therefore consider a mechanistic interpretation of production-resource relationships that we propose provides some insight on these apparent challenges with Michaelis-Menten-based formulations. We begin by considering two fundamentally different light-limited experimental conditions and then draw parallels between these responses and nutrient-limited experimental data to ultimately build a diffusion-focused expression appropriate for describing phytoplankton growth in natural communities.

Let us first consider the familiar experimental procedure of determining 'Photosynthesis-Irradiance' relationships (i.e. a '*P-I* curves'), whereby samples from a phytoplankton population acclimated to a given growth irradiance (I_g, mol quanta m^{-2} d^{-1}) are exposed to a range of light levels (I_E, mol quanta m^{-2} d^{-1}) for a sufficiently brief period that physiological acclimations are negligible. Resultant *P-I* curves (e.g., Fig 2A) are characterized by an initial linear increase in photosynthesis that is defined by photon flux, the number of absorbing (pigment) targets, and the functional absorption cross-section per target. At higher light intensities, the rate of photon capture begins to approach the cell's capacity to utilize the light-driven production of ATP (adenosine triphosphate) and reductant (nicotinamide adenine dinucleotide phosphate, NADPH). This capacity, which defines the maximum (light-saturated) rate of photosynthesis (P_m), is ultimately determined (primarily) by turnover of the Calvin-Benson-Bassham Cycle [23–28]. The value of P_m varies with growth conditions, but its maximum is an evolutionarily-selected property aligned with a given species' maximum division rate (μ_m). Thus, *P-I* curves are defined by a physical process (photon capture) and a biological limit (P_m) and, logically, traditional equations describing these curves are formulated in these terms, such as [29]:

$$P = P_m \, tanh\left(\frac{\alpha_P I_E}{P_m}\right), \tag{5}$$

where the slope, α_P, is the photon capture efficiency at low light [m^2 (mol quanta)$^{-1}$]. *P-I* expressions, such as Eq 5, yield relatively abrupt transitions between light-limited and light-saturated photosynthesis and commonly provide a suitable fit to observational data (e.g., Fig 2A). An 'emergent property' of *P-I* curves is the light saturation index, $I_K^P = P_m / \alpha_P$. For the hyperbolic tangent model (Eq 5), $P = 0.76 \, P_m$ when $I_g = I_K^P$.

In a similar manner to a *P-I* curve, cell division rates (μ, d^{-1}) can be measured across populations acclimated to different growth irradiances (i.e., a 'μ-I_g' curve). Emergent μ-I_g curves are again saturating functions of light level (Fig 2B), but these relationships differ significantly from *P-I* curves because each population has had sufficient time to optimize its physiology according to its growth conditions. This optimization involves the tuning of a plethora of cellular properties, including investments in photosynthetic machinery, nutrient uptake systems, and respiratory pathways. While generalized models of this acclimation process have been
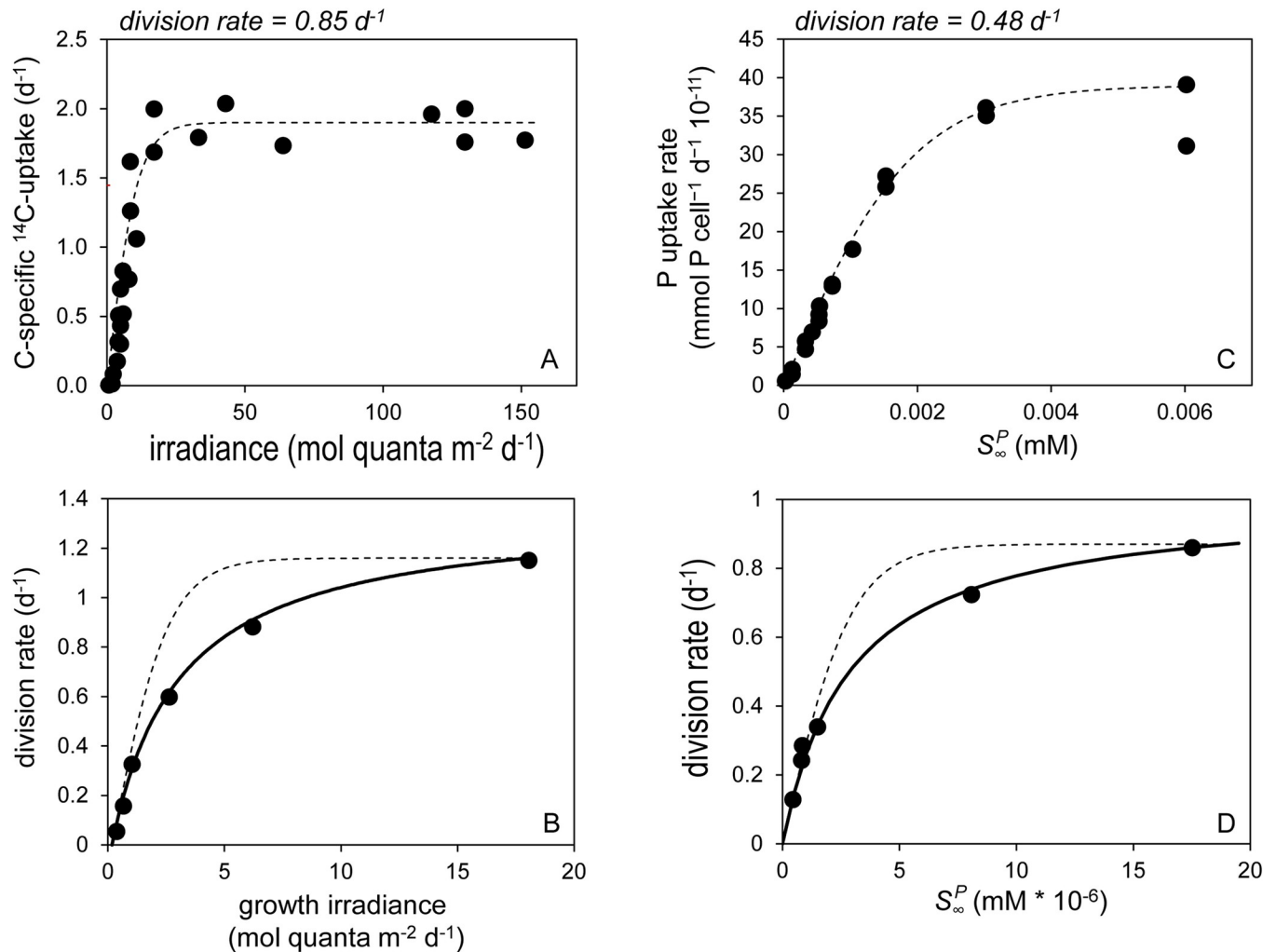
Fig 2. Short-term and acclimated production-resource relationships for light-limited and nutrient-limited phytoplankton populations. (A) Short-term (20 minute) carbon-specific ^{14}C uptake as measured by Fisher & Halsey [76] for *Thalassiosira pseudonana* (Hustedt) Hasle et Heimdal (CCMP 1355) cultures acclimated to a light-limited growth rate of 0.85 d^{-1}. Dashed line = fit of Eq 5. (B) Cell division rates observed by Laws & Bannister [54] for *Thalassiosira weissflogii* (previously, *Thalassiosira fluviatilis*) acclimated to a range in growth irradiance (I_g, x-axis). Solid line = fit of Eq 6. Dashed line = application of Eq 5. (C) Short-term (8 minute) PO$_4$ uptake (atto-mol = 10^{-15} mmol) measured by Laws et al. [55] for *Pavlova lutheri* (Droop) J.C. Green maintained in chemostats at a PO$_4$-limited growth rate of 0.48 d^{-1} and then rapidly exposed to a range of concentrations (x-axis). Dashed line = fit of Eq 7. (D) Cell division rates observed by Laws et al. [32] for *Tetraselmis suecica* (Kylin) Butcher in steady-state PO$_4$-limited chemostat cultures. Solid line = fit of Eq 8. Dashed line = application of Eq 7. (c,d) x-axis = measured far-field PO$_4$ concentration (S_∞^P).

developed [e.g., 30], we currently do not have adequate knowledge on evolutionary histories and life strategies to *a priori* predict the unique 'solutions' expressed by different species. What we can say is that observed μ-I_g curves are again well described (solid black line Fig 2B) as functions of the physical process of photon capture efficiency at low light [α_μ, m^2 (mol quanta)$^{-1}$] and a species-specific biological limit on μ_m (d^{-1}) at high light. However, μ-I_g relationships generally follow a rectangular hyperbolic form that can be expressed as [modified from 31]:

$$\mu = \frac{\alpha_\mu(I_g - I_r)\mu_m}{\alpha_\mu(I_g - I_r) + \mu_m},$$

(6)

where I_r (mol quanta m^{-2} d^{-1}) is the light level at which primary production equals the

maintenance respiration rate [see Note 3 in S1 File]. The significant influence of cellular optimization on the μ-I_g relationship is reflected in Fig 2B by the poorness of fit when Eq 5 is applied to the data (dashed line). For μ-I_g data, an 'emergent' light saturation index can again be defined as $I_K^\mu = \mu_m/\alpha_\mu$, but in the case of the rectangular hyperbolic (Eq 6), $\mu = 0.5\,\mu_m$ when $I_g = I_K^\mu + I_r$.

Production-resource relationships for nutrient-limited populations exhibit very similar properties as light-limited systems. For example, Laws et al [32] exposed cells from a steady-state phosphate-limited population of the haptophyte, *Pavlova lutheri*, growing at $\mu = 0.48$ d^{-1} to a range of phosphate concentrations (S_∞^p) and measured short-term (8 minute) uptake rates (v, mmol cell^{-1} d^{-1}). Analogous to Eq 5, the observed uptake-substrate (v-S_∞) curve is well described by (Fig 2C):

$$v = V_m\ tanh\left(\frac{\alpha_v S_\infty}{V_m}\right),\qquad(7)$$

where α_v (dm^3 d^{-1} cell^{-1}) is an initial slope (akin to α_P) defined by the physical flux of nutrients to the cell surface (i.e., diffusion through the cells boundary layer) and capture by membrane transporters (the 'targets'), while V_m is the nutrient-saturated maximum uptake rate (mmol cell^{-1} d^{-1}). As noted by Laws et al [32] and later by Flynn et al. [33] for nitrogen-limited cultures of *Emiliania huxleyi* and *Heterosigma carterae*, v-S_∞ data are often not well fitted by a rectangular hyperbolic function. Because such data are collected on time scales too short for physiological acclimations, v-S_∞ curves reflect cell uptake capacities for essentially a fixed population of membrane transporters and, thus, can be mechanistically described by so-called 'diffusion-porter' models [33–37].

Modeling steady-state nutrient-limited phytoplankton division rates, on the other hand, requires a description of performance as a function of resource availability (S_∞) akin to a μ-I_g relationship. Here again, optimization of growth results from tuning a plethora of cellular processes (not simply those associated with nutrient uptake and assimilation) and observed relationships reflect evolved 'solutions' specific to each species that, again, we currently do not have sufficient mechanistic understanding of to accurately predict *a priori*. Nevertheless, μ-S_∞ relationships commonly follow a saturating rectangular hyperbolic form [see Note 4 in S1 File] (e.g., Fig 2D):

$$\mu = \left(\frac{\alpha_v S_\infty V_m}{\alpha_v S_\infty + V_m}\right)\frac{1}{Q} = \mu_m\left(\frac{\alpha_v S_\infty}{\alpha_v S_\infty + V_m}\right),\qquad(8)$$

where α_v (dm^3 d^{-1} cell^{-1}) is, in this case, the slope of uptake versus substrate concentration (mM) for populations acclimated to low nutrient levels, Q is the cellular requirement for limiting nutrient (mmol cell^{-1}), and $\mu_m = \frac{V_m}{Q}$. As in Fig 2B, Eq. 7 does not provide a suitable fit to μ-S_∞ data (dashed line in Fig 2D), again illustrating the significant influence of cellular optimization in acclimated populations.

A take-home message of the foregoing discussion is that short-term and acclimated production-resource relationships for both light-limited and nutrient-limited conditions can be logically described as functions of a largely physically-defined flux-capture process (i.e., the α terms) and an evolutionarily selected for, species-specific maximum division rate or related biological property (i.e., V_m. P_m). However, the shapes of short-term and acclimated production-resource relationships differ because of the many physiological 'knobs' cells can turn in the process of optimization. The outcome of this optimization for nutrient-limiting conditions is a production-resource response that typically follows a rectangular hyperbolic form where the saturation index, V_m/α_v, corresponds to the nutrient concentration where $v = 0.5V_m =$

K_m^{cell}. Accordingly, the right hand side of Eq 8 can be reorganized by multiplying the numerator and denominator by $\frac{1}{\alpha_v}$ and substituting $V_m/\alpha_v = K_m^{cell}$ to give:

$$\mu = \left(\frac{\alpha_v S_\infty V_m}{\alpha_v S_\infty + V_m}\right)\frac{1}{Q} = \left(\frac{S_\infty V_m}{S_\infty + \frac{V_m}{\alpha_v}}\right)\frac{1}{Q} = \mu_m\left(\frac{S_\infty}{S_\infty + K_m^{cell}}\right), \tag{9}$$

where the bracketed term of the right-most expression is now the Michaelis-Menten form commonly employed in contemporary plankton ecosystem models (e.g., Eq 4). Here, we have used the term, K_m^{cell}, to acknowledge that this evolved property of optimized whole-cell physiology should not be mechanistically thought of as equivalent to the K_m of a Michaelis-Menten single enzyme-substrate-product reaction.

We propose that, when thinking about nutrient-limited phytoplankton growth in nature, Eq 8 has a distinct advantage over its converted Michaelis-Menten form in Eq 9 (and similarly Eq 4), despite their mathematical equivalence. Specifically, the Michaelis-Menten form is often interpreted as specifying competitive advantages/disadvantages between phytoplankton species because V_m and K_m^{cell} are both viewed as species-specific physiological 'traits'. While this certainly is the case for V_m and a high V_m can bestow an advantage under elevated resource conditions, the limit on K_m^{cell} is primarily dictated by the physical process of diffusion. As such, the common assignment of K_m^{cell} as a metric of nutrient 'affinity' ['*an attractive force between substances or particles*' (Merriam-Webster, https://www.merriam-webster.com/dictionary/)] is misleading, as cells cannot 'attract' resources beyond diffusional limits [for a given morphology, relative motion, and assuming equal efficiency in capturing nutrients at the rate they arrive at the cell surface (see below)]. When individuals are as distantly spaced as in natural populations (Fig 1), their influence on the nutrient field is constrained to their respective boundary layers (outer circles and red arrows in Fig 1C) and has no immediate impact on the far-field (S_∞) experienced by neighboring cells. So long as the phytoplankton of such a community are consumed and their nutrients recycled at a rate equivalent to population uptake (i.e., steady-state conditions), S_∞ remains unchanged and there is, on average, no direct competition between cells, nor does the higher uptake per unit cell volume of smaller phytoplankton directly diminish the uptake and growth of larger cells (we use the term 'directly' here because the standing stock of a given phytoplankton type has an indirect influence on other phytoplankton by influencing S_∞, as we previously discussed and expand upon below). The key point is that, in nature, a species with a low K_m^{cell} does not have an ability to draw down S_∞ such that it can competitively exclude other species with higher K_m^{cell}. However, this is generally not the case in laboratory competition experiments [e.g., 22] where high cell concentrations result in frequently overlapping boundary layers, resulting in direct competition and subsequent exclusion [12].

In the previous section, we painted a picture of the phytoplankton world highlighting the discreteness of individual cells. We then asked whether traditional formulations for phytoplankton growth (Eq 4) found in contemporary ecosystems models are flawed because they treat phytoplankton populations as continuous fields of an elemental stock, rather than as discrete entities [see also 12]. In the current section, we discuss the basis of observed production-resource relationships and provide an expression (Eq 8) for nutrient-limited growth of distantly-spaced, non-competing phytoplankton. For a population of equally-sized cells, this equation yields the same prediction for steady-state biomass when implemented at the individual level and then integrated over the population as when implemented at the integrated population level. For a population of polydispersed cells, the outcome of Eq 8 is likewise the same for these two implementation approaches so long as size-dependences in diffusion are

accounted for. As Eq 8 is mathematically equivalent to a Michaelis-Menten form, *our conclusion is that there is nothing fundamentally incorrect about applying relationships such as Eq. 4 when modeling distantly spaced phytoplankton.* Ironically, what may be missing from such equations is, instead, a term accounting for competition under conditions when cells are in close proximity.

If the fore-stated conclusion is valid, then where have previous interpretations gone wrong? We propose that the answer to this question is two-fold. First and as noted above, the thought of K_m^{cell} as a species-specific 'affinity' acting to deplete S_∞ is incorrect and should be replaced by a view that K_m^{cell} is an 'emergent property' of size-dependent diffusion processes, species-specific μ_m, and evolved optimization strategies. Second, previous interpretations of Eq 4 are incorrect; specifically, the conclusion that treating phytoplankton biomass as an integrated elemental stock is equivalent to a continuously distributed fluid variable. The fact is that there is nothing about Eq 4 that explicitly states how biomass is spatially distributed, only that it has an integrated mass. If information on the size of cells within this mass is retained, then appropriate diffusion rates can be applied in calculating growth rates, irrespective of the spacing between individuals.

The above insights help reconcile earlier conceived issues, but they also make the original problem motivating this study even more vexing. If current expressions in ecosystem models are consistent with growth in a competition-neutral resource landscape [19, 21] (i.e., a landscape where resource attainment by some species does not lead to competitive exclusion of others), then why do these models yield extinctions of most phytoplankton size groups under oligotrophic conditions? As a first step toward answering this question, we will now explore the size distribution of phytoplankton division rates from a diffusion-focused perspective.

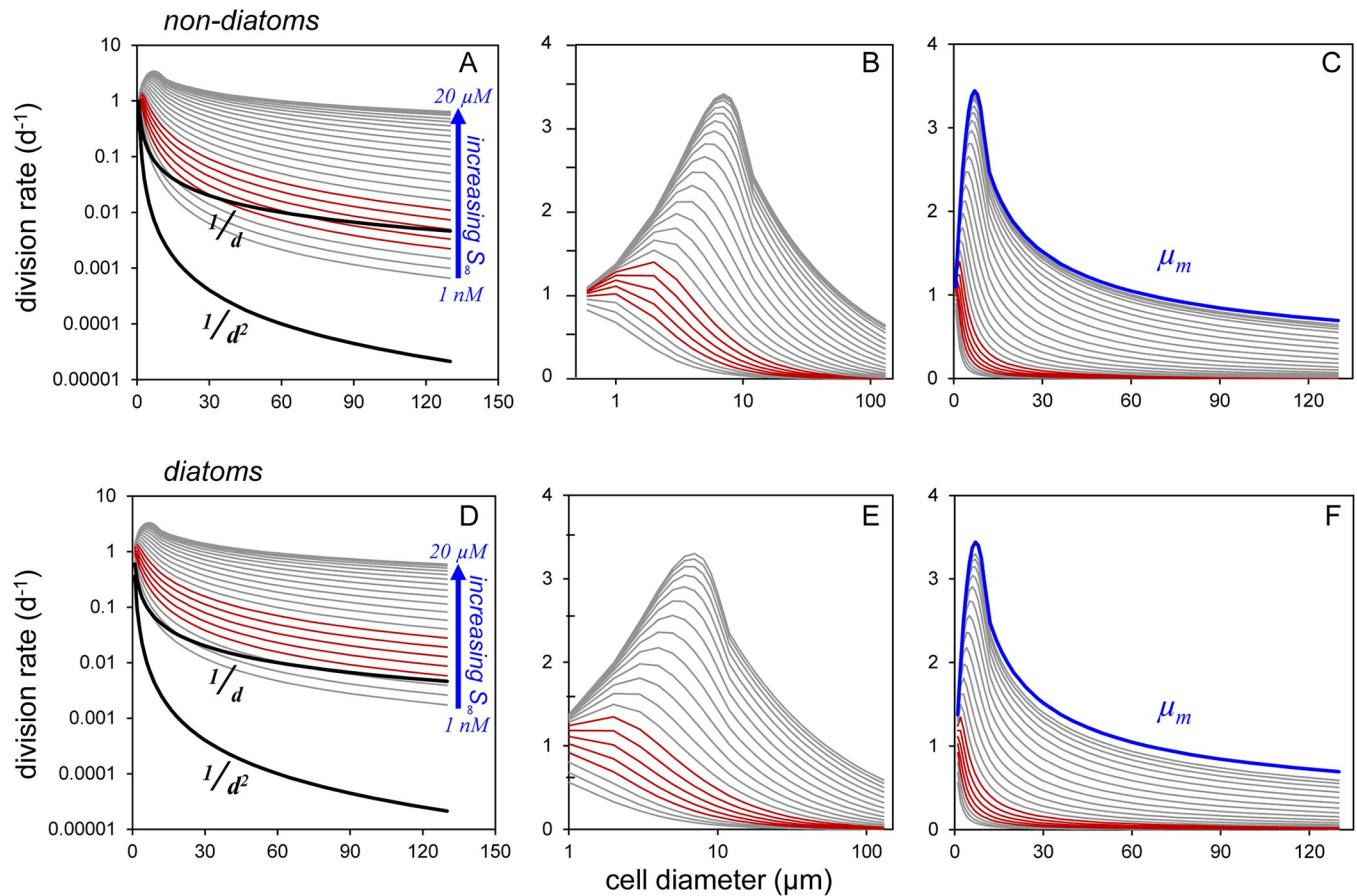## Diffusion-supported phytoplankton division rates

The diffusional flux of nutrients to the surface of a phytoplankton cell is dependent on a variety of factors, including cell size and shape, movement (e.g., sinking, swimming) relative to the surrounding medium, and the efficiency with which transporter proteins translocate nutrients across the cell membrane relative to the diffusive rate at which they arrive at the membrane [this relative rate determines the concentration gradient between the cell surface (S_0) and S_∞]. Here, we will forgo a detailed description of molecular diffusion and, instead, refer interested readers to the rich literature that already exists describing solute flux across cell boundary layers [e.g., 38–42]. For simplicity, we will assume that phytoplankton are spherical cells, such that the diffusional flux (F_D) to the cell surface in the absence of relative motion is described by:

$$F_D = 4\pi\left(\frac{d}{2}\right)D(S_\infty - S_0) \approx 2\pi dD S_\infty, \tag{10}$$

where d is cell diameter, D is the diffusion coefficient for a given nutrient type, and the rightmost expression assumes that the cell is a perfect absorber (i.e., $S_0 = 0$). Eq 10 states that the nutrient flux to a phytoplankton scales with cell diameter. Accordingly, the cell-volume-specific flux (F_D') for a spherical cell is:

$$F_D' \approx \frac{2\pi dD S_\infty}{\frac{4}{3}\pi\left(\frac{d}{2}\right)^3} = \frac{3DS_\infty}{\left(\frac{d}{2}\right)^2}, \tag{11}$$

which predicts that, if growth rate is limited purely by diffusion, the size-distribution of division rates will not scale in proportion to the surface:volume ratio (i.e., $1/d$; upper heavy black lines in Fig 3A, 3D) but rather with the inverse square of cell diameter (i.e., $1/d^2$; lower heavy

Fig 3. Diffusion-supported phytoplankton division rates as a function of cell size predicted for a range in far-field nutrient concentrations (S_∞) reflective of highly oligotrophic to highly eutrophic natural waters. (A-C) Non-diatoms. (D-F) Diatoms. (A,D) Lower heavy black line = initial prediction for diffusion-limited growth at all cell sizes. Upper heavy black line = division rate prediction if following cellular surface:volume ratios. Grey lines = size-dependent division rates for S_∞ ranging from 1 nM to 3 μM (blue labeling). Red lines = division rates for biologically-available nitrogen concentrations of 3 nM to 17 nM typical of S_∞ values in oligotrophic ocean gyres. (B,E) Same data as in left column but with normal y-axis and log-transformed x-axis to better reveal size-dependent division rates of small cells. (C,F) Same data as in left column but with normal axes. Blue line = envelope in size-dependent maximum division rates (μ_m) from Behrenfeld et al. [53].

black lines in Fig 3A, 3D) [41]. To place this initial prediction in context, *it implies that a nutrient-limited 1 μm cell will be dividing 10,000 times faster than a nutrient-limited 100 μm cell.* Clearly, this prediction is inconsistent with reasonable size-dependent changes in μ for natural populations [43]. Nevertheless and as noted by Jumars et al. [39], even large cells are limited in their ability to alleviate this strong constraint of diffusion through their relative motions or morphological adaptations [see also 40].

Resolution of the above issue emerges by combining estimates of diffusional flux (Eq 10) with a μ-S_∞ relationship (Eq 8) for nitrogen-limited growth. In oligotrophic ocean regions, surface layer ammonium (NH_4) concentrations commonly range from <3 nM (i.e., detection limit) to 10's of nM, while summed nitrate and nitrite levels range from undetectable to slightly less than 10 nM [44–48, https://hahana.soest.hawaii.edu/hot/hot-dogs/interface.html]. In more productive ocean regions, available nitrogen sources can exceed μM concentrations [49]. We therefore consider here far-field nitrogen concentrations of 1 nM $\leq S_\infty^N \leq$ 20 μM.

Cell division rates over our range in S_∞^N were determined for diatoms of diameter 1 to 130 μm and for other phytoplankton over the size range 0.6 to 130 μm. The diffusional flux of

nutrient was calculated from Eq 10 assuming $S_0 = 0$ and a constant $D = 1500$ μm^2 s^{-1} (i.e., ignoring, for example, effects of temperature). The influence of relative motion on F_D was estimated by first calculating a size-dependent characteristic velocity ($\mathcal{U}$; μm s^{-1}) for swimming by non-diatoms ($\mathcal{U}_{swimming}$) following [50, see Note 5 in S1 File]:

$$\mathcal{U}_{swimming} = [93(d/10000)^{0.26}]\, 10000 \tag{12A}$$

and for sinking ($\mathcal{U}_{sinking}$) in diatoms of $d \geq 8$ μm (i.e., $\mathcal{U}_{sinking} = 0$ for $d < 8$ μm) based on data from Waite et al. [51; their Fig 7A]:

$$\mathcal{U}_{sinking} = \left[0.0007\, ln\left(\frac{d}{20000}\right) + 0056\right] 10000. \tag{12B}$$

Péclet numbers (P_e) for both phytoplankton groups were then calculated as:

$$P_e = \frac{d\mathcal{U}}{D} \tag{13}$$

and used to assess Sherwood numbers (Sh) following [40]:

$$Sh = \frac{1}{2}\left(1 + (1 + 2P_e)^{1/3}\right), \tag{14}$$

where Sh quantifies the enhancement in diffusive flux relative to F_D of a non-moving cell (Eq 10). Finally, Jumars et al. [39] evaluated the relationship between membrane transporter abundance and the fraction of F_D captured by a cell. Their analysis revealed a remarkable efficiency [also see 52], such that less than 0.1% of a membrane needs to be occupied by transporters to collect ~50% of the diffusive flux. Here, we will assume a 90% capture efficiency, which would correspond to ~1% membrane coverage [39; their Fig 3]. The *potential* nutrient flux available for assimilation (A_F) is thus:

$$A_F = 0.9\, Sh\, F_D, \tag{15}$$

which can be substituted in Eq 8 as $A_F = \alpha_v S_\infty^N$.

To calculate division rate (Eq 8), a size dependent estimate of V_m is needed. In an earlier study [53], we found that measured maximum division rates (cell doublings per day) reported in the literature fall within an upper envelope that increases with cell size up to $d \sim 7$ μm and then decreases with size in a manner following a power function at $d \geq 15$ μm. This envelope is described by (upper blue curves in Fig 3C, 3F):

$$\mu_m = [-0.0555(d)^2 + 0.789d + 0.64]\, ln(2) \qquad (\text{for } d < 15\ \mu m) \tag{16A}$$

and

$$\mu_m = [9.29(d)^{-0.533}]ln(2) \qquad (\text{for } d \geq 15\ \mu m), \tag{16B}$$

where multiplication by $ln(2)$ in each equation coverts maximum doublings per day [reported in 52] to maximum specific division rates (μ_m, d^{-1}). As V_m (fg N $cell^{-1}$ d^{-1}) is the rate of nutrient uptake (in this case nitrogen) required to support μ_m, it can be estimated as the product of cellular carbon and the nitrogen:carbon ratio at μ_m ($N{:}C_m$):

$$V_m = 1000\, N : C_m C \mu_m, \tag{17}$$

where C (pg C $cell^{-1}$) was calculated following Menden-Deuer & Lessard [20] as stated above for non-diatoms and as $C = 10^{-0.541 + 0.811 Log_{10}(Vol)}$ for diatoms, $N{:}C_m$ was estimated from $N{:}C = 0.0762\mu + 0.0389$ based on Laws & Bannister [54; their Table 1 for nutrient-limited

cultures], and the scalar, 1000, converts C in pg C cell^{-1} to fg C cell^{-1}. Application of Eqs 15 and 17 in the rectangular hyperbolic element of Eq 8 yields the nutrient assimilation rate for a given cell size and S_∞^N. Relating this rate to μ requires accounting for growth-rate-dependent changes in nutrient requirements specified by our equation for $N{:}C$. Realized division rates for each value of S_∞^N were thus determined by first calculating the division rate that is supported by a given assimilation rate, assuming $N{:}C = N{:}C_m$, and then iteratively adjusting $N{:}C$ and μ from this initial estimate until stable values were achieved. For all combinations of cell size and S_∞^N, this stabilization was achieved within 25 iterations.

The outcome of the above formulations is shown in Fig 3 for non-diatoms (top) and diatoms (bottom), where the left panels are plotted with a log-transformed y-axis, the center panels with a log-transformed x-axis, the right panels with normal axes, and in all panels typical oligotrophic conditions of 3 nM $\leq S_\infty^N \leq$ 17 nM are indicated by red lines. A key finding here is that size spectra for phytoplankton division rates fall far from a scaling with the square of cell diameter ($1/d^2$), as initially predicted, when based on diffusion for realistic S_∞^N and they even lie above a surface:volume dependence ($1/d$) for all but the lowest S_∞^N. The reason for this is that the diffusional potential (A_F) for small cells is close to or exceeds that necessary to support μ_m even at very low S_∞^N, such that any residual changes in μ with increasing nutrient supply simply reflect the slowly-saturating nature of evolutionarily-optimized μ-S_∞ relationships (e.g., Fig 2D). Because the steady-state biomass of a given phytoplankton size class is determined by μ-dependent predator-prey relationships, expectations from these results when applied to an ecosystem model are an even further dampening in the range of equilibrium biomasses across size classes (compared to the range in size-dependent μ) at low nutrients and a much stronger potential for proliferation of large species with increasing S_∞^N, which will tilt the size distribution slope upward toward -3 [19].

In the next section, we will apply our diffusion-focused approach in a modified version of a published ecosystem model, but before proceeding we conclude the current section with a comparison of our modeled μ values and observational data from two chemostat-based studies where measurements of S_∞ were reported [32, 55] to evaluate if our formulation provides reasonable predictions. In the first of these studies, phosphate-limited cultures of the temperate chlorophyte, *Tetraselmis suecica*, were maintained at steady-state division rates of ~0.16 to ~0.75 d^{-1}, which corresponded to S_∞^P concentrations ranging from ~0.7 to ~5.6 nM, respectively. Applying our above-described diffusion-based approach for an average *T. suecica* cell diameter of 12 μm, a cellular elemental nitrogen:phosphate ratio ($N{:}P$) of 16:1, and a μ_m of 1.2 d^{-1} [32] yields estimates of μ that are highly consistent ($R^2 = 0.96$) with observed values (Fig 4A). This finding implies an optimization strategy in *T. suecica* aimed at fully utilizing the diffusional flux of limiting nutrient to the cell surface. In the second study [55], phosphate-limited cultures of the temperate haptophyte, *Pavlova lutheri*, were maintained at steady-state division rates ranging from ~0.13 to ~0.85 d^{-1}, with corresponding S_∞^P values of ~0.4 to ~17.5 nM, respectively. In this case, application of our diffusion-based approach for an average *P. lutheri* cell diameter of 6 μm, a $N{:}P$ of 16:1, and a μ_m of 1.0 d^{-1} [55] yields correlated ($R^2 = 0.97$) but somewhat overestimated values of μ compared to observations (Fig 4B) [note that these same data are very well fitted by an empirically-parameterized version of Eq 8 (Fig 2D)]. Perhaps the observed modest departure from pure diffusion limitation observed in *P. lutheri* implies that the evolved life strategy of this species involves other tactics for success aside from maximizing nutrient utilization. In this regard, it might be noted that the cultured isolate, *P. lutheri* (Droop) Green, was originally obtained from an intertidal location of the Clyde Sea where one might speculate that selection pressures may have been weak for success under low nutrient conditions and perhaps more oriented toward defense (grazer or other) strategies.
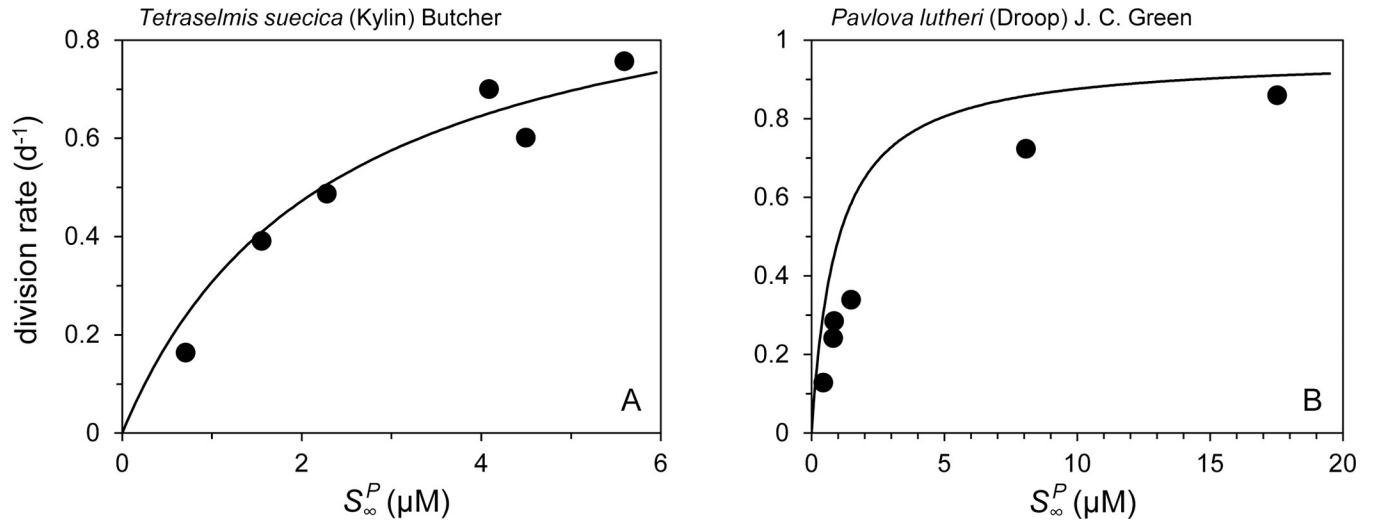
Fig 4. Comparison of model-predicted phytoplankton division rates with measure steady-state rates in PO₄-limited chemostat cultures. (A) Circles = cell division rates observed by Laws et al. [32] for *Tetraselmis suecica* (Kylin) Butcher. Solid line = predicted division rates assuming an average cell size of 12 μm and a maximum division rate (μ_m) of 1.19 d⁻¹ [32]. (B) Circles = cell division rates observed by Laws et al. [55] for *Pavlova lutheri* (Droop) Green. Solid line = predicted division rates assuming an average cell size of 6 μm and a μ_m of 0.98 d⁻¹ [55].

One-dimensional ecosystem model

Ecosystem modeling can be a bit of an 'art form' in terms of tuning parameters to achieve stable and reasonable results (i.e., when compared to observations) [12, 56] and as the complexity of a model increases, understanding its behavior becomes more difficult [57, 58]. Given the findings described in the previous sections, the intention of the following exercise was to resolve our initial question regarding why contemporary ecosystem models often yield significant extinctions of larger phytoplankton species under steady-state low-nutrient concentrations, whereas field observations indicate the coexistence of a continuum in phytoplankton sizes. Accordingly, we have chosen here to employ the following minimal equation set such that a clear answer to this question emerges:

$$\frac{dP^N}{dt} = \sum_{i=1}^{i=j} (\mu_i P_i^N - g_1 f_i Z_i^N P_i^N) \tag{18A}$$

and

$$\frac{dZ^N}{dt} = \sum_{i=1}^{i=j} (g_1 g_2 f_i Z_i^N P_i^N - g_3 Z_i^N - g_4 f_i (Z_i^N)^2) \tag{18B}$$

where P_i^N is the total nitrogen inventory (mmol m⁻³) of the ith phytoplankton size class, phytoplankton mortality is solely due to grazing, Z_i^N is the nitrogen inventory of the zooplankton population (mmol m⁻³) with a grazing range centered on the ith phytoplankton size class, μ_i is the diffusion-supported division rate (d⁻¹) for a given S_∞^N (calculated as described in the previous section), and f_i introduces flexible feeding by predators over a range of prey bin sizes (defined below). Parameters g_1 through g_4 represent zooplankton grazing rate, ingestion efficiency, non-grazing mortality rate, and density-dependent mortality rate, respectively, and are assigned size-independent values of g_1 = 3.24 m³ mmol⁻¹ d⁻¹, g_2 = 0.5 (unitless), g_3 = 0.06 d⁻¹, and g_4 = 1.6 m³ mmol⁻¹ d⁻¹ [59].

The size structuring of our modeled ecosystem generally follows that described for the "*idealized food-chain model*" developed by Ward et al. [10]. Our 'baseline' model is executed for the nutrient-limited growth rates of either non-diatoms or diatoms and includes 25 phytoplankton size-classes with diameters ranging from 0.6 μm to 135 μm, where cells in a given size class are 1.25 times larger than those in the class one size smaller (i.e., $d_i = 0.6 \times 1.25^{i-1}$). The model also includes 25 zooplankton size classes that graze on a range of phytoplankton sizes. The feeding size range consumed by predators of phytoplankton and zooplankton is assumed proportional to (f_i in Eqs 18A,18B) their mean prey size (e.g., in the current case we define f_i = ([d_i+0.5d]—[d_i-0.5d]) / 1 μm, meaning that a predator with a mean prey size of 100 μm will have a feeding range of 50–150 μm, while a predator with a mean prey size of 2 μm will have a feeding range of 1–3 μm) [10, 19, 60]. Because our focus is on phytoplankton size composition under steady-state (in this case, nitrogen-limited) growth conditions, we do not consider the role of environmental variability. For each model run, S_∞^N is held constant at a value between 1 nM and 20 μM (stepped every 7 nM between 1 and 35 nM and every 200 nM thereafter) and light levels are assumed constant and saturating for growth. Because S_∞^N is held constant, phytoplankton nitrogen consumed but not assimilated by grazers and grazer nitrogen lost to linear and density-dependent predation are removed from the modeled system and not recycled (as in [10]). Model runs for each S_∞^N are initiated with P_i^N = 0.18 mmol N m⁻³ and Z_i^N = 0.04 mmmol N m⁻³ for all size classes and then executed for 3 years at ~15 minute time-steps (noting that the 3-year time frame was conservative as actual times for all phytoplankton size classes to reach equilibrium was only 30 days to ~1.5 years, with the longer times required for lower values of S_∞^N) [see Note 6 in S1 File]. Size diversity for the steady-state populations was assessed as the number of 'species' (i.e., size-classes) remaining that contributed at least 0.0001% to total phytoplankton biomass [see Note 7 in S1 File].

The first and most important result from our ecosystem model is that all phytoplankton size classes are retained under all values of S_∞^N for both our non-diatom and diatom communities (Fig 5A, red & yellow line). This finding contrasts starkly with results from earlier ecosystem models where only the smallest species persist at low S_∞^N [e.g., 4–6]. This difference may seem rather surprising given our earlier statement that the diffusion-focused expression for μ (Eq 8) can be re-cast in a Michaelis-Menten form consistent with earlier ecosystems models (Eq 9) and that our model equation set (Eqs 18A,18B) is little altered from even the pioneering work of Riley [61] and Evans & Parslow [57]. The reason for our sustained biodiversity is revealed below, but first it is useful to directly compare our findings with predictions from a previously published and very similar ecosystem model (noting here that this comparison is simply for illustrative purposes and is in no way intended to criticize the earlier model).

The Ward et al. [10] "*idealized food-chain model*" was developed as a simplistic model to better understand the behavior of a more complex "*global food-web model*" [60]. The simpler model (the code for which was kindly provided by B. Ward for developing our current model) was intended to mimic a chemostat system [thus, it included terms for new media input, outflow of both culture media and associated phytoplankton, and did not recycle nutrients (as in our model)] and, importantly, yields a prediction of phytoplankton diversity as a function of nutrient availability that is fundamentally equivalent to the fully coupled *global food-web model* [60]. The Ward et al. [10] plankton equations differ from our approach (Eqs 18A,18B) in that they (1) include non-grazing phytoplankton mortality terms (cell death and culture outflow = 0.03 d⁻¹), (2) a light/temperature-limitation term, and (3) lack a density-dependent zooplankton predation term. The Ward et al [10] model also assumes that all small cells are non-diatoms and all large cells are diatoms. Each phytoplankton and zooplankton size class is initiated with a biomass of 10^{-10} mmol N m⁻³, which may then increase as nutrients are added
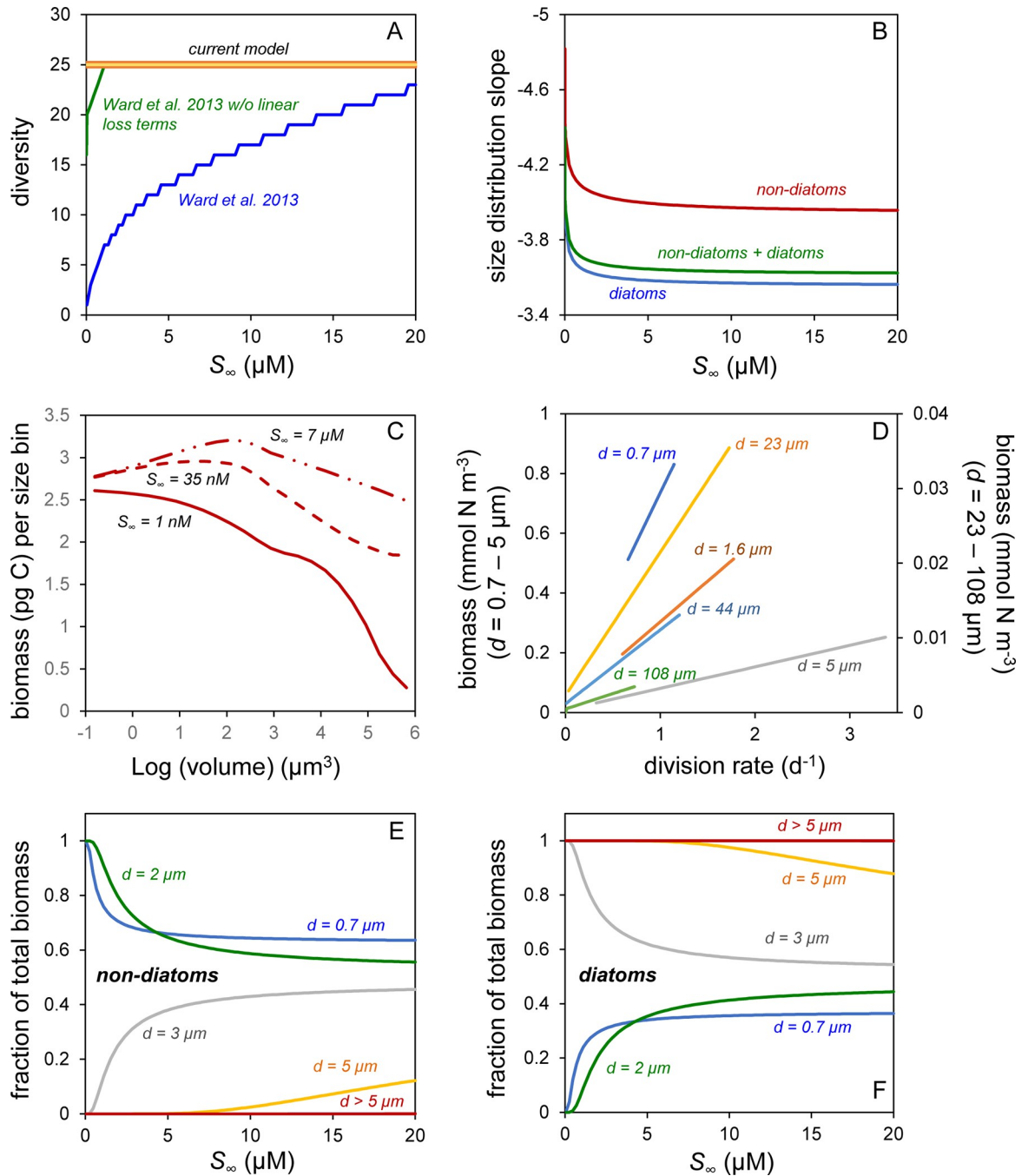
Fig 5. Properties of model-based steady state phytoplankton communities. (A) Phytoplankton diversity as a function of far-field nutrient concentration (S_∞) for model runs initiated with 25 distinct 'species' (size classes). Heavy red line, thin yellow line = Non-diatom and diatom diversity for ecosystem model developed herein, respectively. Blue line = Phytoplankton diversity predicted by the Ward et al. [10] model. Green line = Diversity predicted by Ward et al. [10] model but with non-grazing loss terms (m, κ) omitted. (B) Phytoplankton size distribution slopes (SDS) for the linear relationship between the logarithm of cell number concentration per unit length and logarithm of cell diameter as a function of S_∞. Colors = Model runs for non-diatom, diatom, and mixed communities. (C) Examples of the shift in dominance from small cells to large cells as the SDS increases with increasing S_∞ (labeled next to line). Data are for non-diatom cell types where abundance and cell volume data values are converted to biomass following Menden-Deuer & Lessard [20]. (D) Relationships between phytoplankton division rates and biomass for cell diameters ranging from 0.7 to 108 μm. Left axis = Results for cell diameters ranging from 0.7 to 5 μm. Right axis = Results for cell diameters ranging from 23 to 108 μm. (E) Fraction of total phytoplankton biomass from the multispecies model runs that is attributable to different size classes of non-diatoms and as a function of S_∞. Modeled size classes ranged from 0.7 to 135 μm, but non-diatoms only contributed significantly to total biomass at cell diameters below ~5 μm. (F) Same as in (E) except showing results for diatoms.

to the model system. For the current comparison, we executed the Ward et al. [10] model as originally published except with the light/temperature-limitation term removed. Predicted steady-state phytoplankton diversity from this model is shown by the blue line in Fig 5A, which is essentially identical to the result presented in Fig 4A of Ward et al. [10]. The model outcome is that only one or a few species (the very smallest size classes) are sustained at the lowest values of S_{∞}^{N} and then diversity slowly increases (additional larger species are retained) with increasing nutrient inputs.

The loss of steady-state diversity at low S_{∞}^{N} in the Ward et al. [10] simulations is consistent with other fully-coupled ecosystem models [e.g., 4, 5], but it is not the consequence of resource-based competitive exclusion, as our model employs essentially an equivalent functional form for nutrient-limited phytoplankton division yet maintains all modeled species. Instead, diversity loss in the earlier model is a consequence of the non-grazing phytoplankton loss terms (cell death and chemostat outflow). Specifically, the Ward et al. [10] model is initiated with low concentrations of phytoplankton and zooplankton in all size classes and subsequently the slow division rates of larger phytoplankton at low nutrient levels coupled with constant cell death (m) and media outflow (κ) rates prevent these species from accumulating to a sufficient extent that their biomass crosses even a conservative 'extant versus extinct' threshold (here, 0.0001% of total biomass). Indeed, at low nutrient levels, the non-grazing mortality rates alone can exceed diffusion-limited division rates for species > 20 μm such that, even in the absence of other losses, these phytoplankton groups decrease in biomass if not repeatedly 'restored' to the initial 10^{-10} mmol N m^{-3}. In contrast, nutrient concentrations in our model begin at a predefined S_{∞}^{N} and the non-grazing phytoplankton mortality terms are excluded. The importance of non-grazing mortality as an agent for exclusion in earlier models [4, 5, 10] is revealed when the Ward et al. [10] model is re-run without the m and κ terms, which results in nearly full diversity being sustained at even the lowest S_{∞}^{N} (Fig 5A, green line).

In addition to sustaining size diversity, our 'baseline' model predicts phytoplankton abundances in the smallest size bin (equivalent to *Prochlorococcus*) of ~10^{5} cells ml^{-1} and larger species that follow a phytoplankton size distribution slope that tilts upward (i.e., become less negative) as S_{∞}^{N} increases from 1 nM and 20 μM (Fig 5B). The model range for the size distribution slope and its behavior with S_{∞}^{N} is broadly consistent with field observations [e.g., 15, 17–19] and corresponds to biomass dominance shifting between picophytoplankton and microphytoplankton (Fig 5C). These shifts in community structure are driven by size-dependent potentials for diffusion-driven increases in μ as S_{∞}^{N} increases (Fig 5D), noting here that these relationships are not 1:1 with biomass and reflect predator-prey balances between division and loss rates at equilibrium [59, 62]. These predator-prey balancing points at very low nutrient levels yield a biomass (thus, nutrient sequestration) dominance by very small species because of strong size-dependent changes in μ, but do not result in exclusion of phytoplankton size classes.

Results presented here indicate that our 'baseline' model yields properties of phytoplankton communities reflective of field observations and provides an explanation for the loss of diversity in previous modeling studies. While it is beyond the scope of the current study to fully explore other model parameterizations or constructs, it is hard to resist the temptation to try at least one modification. In particular, what happens when diatoms and non-diatoms are modeled together across all size classes? To answer this question, we modified the baseline model such that each of the 25 phytoplankton size classes had a diatom and non-diatom representative (each initiated with $P_{i}^{N} = 0.18$ mmol N m^{-3}) and we assumed that zooplankton grazers in each size class had no preference for phytoplankton prey types. All other aspects of the model were unaltered. Steady-state size distribution slope solutions for this multispecies model are

shown as a function of S_∞^N in Fig 5B (green line), while the fractional contributions of non-diatoms and diatoms to total phytoplankton biomass in each size class are shown in Fig 5E and 5F, respectively. The multispecies size distribution slopes (Fig 5B, green line) reflect shifts in community composition, with non-diatoms dominating at low S_∞^N and diatoms dominating at high S_∞^N. The reason for this shift is that swimming by non-diatoms proffers a minor advantage over diatoms in terms of diffusive nutrient flux at the smallest cell sizes. In contrast, sinking and cell vacuolation (accounted for in the Menden-Deuer & Lessard [20] relationship) slightly improve nutrient acquisition relative to requirements in large diatoms compared to swimming in unvacuolated non-diatoms. While these differences in diffusive flux are small, they are associated with slight changes in division rate that, when played out over time, result in resounding size-dependent shifts in species dominance (Fig 5E, 5F), a reflection of the 'trophic exclusion principle' discussed in Behrenfeld et al. [21] that can impose strong selective pressure in plankton communities in the absence of resource-based competitive exclusion.

Synthesis

The realm of the phytoplankton can be non-intuitive to large-bodied terrestrial organisms such as ourselves. The number of individual phytoplankton in a waterbody may be astronomical, but from a body-length perspective they are distantly spaced. The tempo of phytoplankton division and death is unfamiliar to us, yet it is of fundamental importance to community structuring and succession. A limiting nutrient may be only a short distance from a cell, but accessing this resource can be challenging because most phytoplankton have a limited capacity to move relative to the water molecules surrounding them. In three previous studies [19, 21, 53], we grappled with developing an understanding of diversity and succession in this foreign world experienced by phytoplankton, and it seemed to us then that a key in doing so would be to explicitly account for the discreteness of individual cells. With this in mind, we undertook the current investigation to model phytoplankton populations from the 'perspective' of a cell, albeit not by modeling individual cells *per se*. Within this perspective, phytoplankton are immersed in a medium where far-field limiting nutrient concentrations are a constant (i.e., assimilation and remineralization rates are balanced), there is no direct resource competition between neighboring cells, and performance of a given species (cell size) is defined by nutrient diffusion across a boundary layer and a physiological optimization strategy that, at sufficient resource supply, supports an evolutionarily-selected maximum growth rate. Our hope was that this approach might help illuminate why extreme competitive exclusion appears to be a common behavior in contemporary ecosystem models.

One of our initial concerns with constraining phytoplankton growth strictly through diffusion limitation was that resultant division rates would unrealistically vary inversely with cell diameter squared [41]. It was therefore satisfying when size distributions in division rate emerged from our semi-empirical model that varied by even less than the surface:volume ratio for nutrient concentrations representative of nearly all natural waters (Fig 3). The reason for this outcome is that, over much of the phytoplankton size domain, realized division rate is governed more by the optimization of cellular machinery than diffusional flux, even at the lowest nutrient levels. In other words, smaller cells are operating in the slowly-saturating region of their μ-S_∞ relationships (Fig 2D) where diffusion potential exceeds utilization [34]. It is noteworthy, here, that our modeled division rates essentially represent an upper limit on growth (if not supplemented by other nutrient sources; e.g., mixotrophy) at low nutrient concentrations that, apparently, some species have evolved to take full advantage of (Fig 4A) and others have not (Fig 4B).

In Behrenfeld et al. [19, 21], we expressed a concern that contemporary ecosystem models encompass an unrealistic degree of resource-based competition between phytoplankton classes, a view earlier shared in Siegel [12]. Our mistake was in envisioning that the modeling of phytoplankton groups simply as integrated elemental stocks was equivalent to treating them as diffuse overlapping fields (i.e., 'fluid variables') where direct competition is continuous. By formulating growth herein as a function of boundary layer diffusion, it seemed to us that a model could be developed that is completely compatible with phytoplankton being discrete entities in a competition-neutral resource landscape. However, in the process of developing this model, we realized that our diffusion-focused equation could be transformed into a mathematically-equivalent Michaelis-Menten form consistent with earlier model formulations. This insight (at least for us) made it clear that direct resource competition is not inherently implied by treating phytoplankton biomass as a fluid variable and that observed extinctions of phytoplankton size classes in ecosystem models cannot simply be interpreted as competitive exclusion by smaller cells with higher nutrient 'affinities'. Indeed, we propose that the common association of nutrient half-saturation values (K_m^{cell}) with 'affinity' has misguided earlier interpretations and that K_m^{cell} is better viewed, going forward, as simply an emergent trait reflecting a size-dependent diffusion constraint and evolved strategies for up-regulating cellular capacities with increasing resource availability. In the discrete world of the phytoplankton, there is rather little a cell can do beyond sinking and swimming to enhance diffusive potential and, even if it could, it generally would have little impact on the far-field nutrient environment experienced by neighbors.

With the above realizations, it became even more intriguing why ecosystem models generally predict low phytoplankton biodiversity in nutrient impoverished regions, a prediction opposite that of observations [63]. By employing our diffusion-governed growth equations in a phytoplankton-zooplankton equation set, we find that the entire size-diversity included in our 'baseline' model at initiation is sustained within the emergent steady-state populations for all far-field nutrient concentrations. Instead of nutrient competition being the cause of exclusions in models, we find that species losses in earlier models for low nutrient conditions are largely attributable to the inclusion of a constant non-grazing phytoplankton mortality rate (d⁻¹) that, as we argue below, is difficult to justify.

There are many facets of plankton ecology that our simple ecosystem model fails to capture. For example, it does not account for competition between individuals when relative motions cause boundary layers to transiently overlap and we don't explicitly account for phytoplankton losses to viral lysis (although, if this process is density-dependent, it might be envisioned as included in the grazing term of Eq 18A). Additionally, our model fails to address the importance of mixotrophy in phytoplankton growth rates [e.g., 33, 64], we do not account for the roles of selective feeding or grazer defense strategies, and we only consider the condition of uniform nitrogen limitation, ignoring the effects of nutrient patchiness [65], potential unique aspects of phosphate, iron, or light limitation, and potential advantages of hosting endosymbionts [66–68]. The benefit of our model equation set is that it is sufficiently simple that predictions can be robustly interpreted, thus following the philosophy of Evans and Parslow [57] and Ward et al. [10]. In the latter study, the simplified equations were not intended to capture the complexities of plankton food webs, but had the important feature of reproducing the loss of species diversity at low nutrient levels exhibited in a fully-coupled global model. Accordingly, we used a similar set of equations to diagnose that the basis for this diversity loss is rooted in non-grazing mortality terms commonly employed in ecosystem models.

An important question that emerges from our study is, if a fixed non-grazing mortality rate for phytoplankton is inappropriate, then how should models capture these phytoplankton losses in the future? The fact is that phytoplankton do die in nature from processes other than

being eaten. For example, stress can lead to programmed cell death [69], viral lysis can behave in a manner that is not density-dependent [70], and other forms of disease and life cycle transitions can result in phytoplankton loss [71, 72]. However, without a mechanistic understanding on how to predict when, where, and to what extent these mortality processes occur, it is difficult to accurately represent them in models [5]. Accounting for these losses by treating them as a constant daily loss rate seems unrealistic and has catastrophic impacts on modeled community diversity [as shown herein and also see 5, 73, 74]. For the model results shown in Fig 5, we omitted the non-grazing mortality term typically found in ecosystem models and this single change allowed all phytoplankton size classes to be sustained at all nutrient levels, however other approaches may also be taken that achieve the same result. As a simple example, if we retain the non-grazing mortality term in our model but assume that this loss rate is a constant per generation rather than per day, then we again sustain the full diversity in phytoplankton sizes at all nutrient levels (i.e., the result is exactly the same as the orange and yellow lines in Fig 5A). Clearly, a fuller understanding of non-grazing mortality rates and their mechanistic relationships to environmental variability are needed to advance ecosystem modeling going forward.

Throughout this manuscript, we have emphasized the role that spatial distancing between phytoplankton cells plays in diminishing potentials for direct resource-based competition. It is important to understand, however, that we are not suggesting that the plankton world is free of competition. Rather, we envision it as a landscape of extreme competition, but one that is largely not based on resource acquisition. Instead, this competition plays out through the interactions of predators and prey. The average life expectancy of an individual phytoplankton in the global ocean is on the order of a day to weeks [75]. Under this rapid tempo of turnover, minor differences in fitness between species result in selection of a finely tuned biodiversity, a process we earlier referred to as the 'trophic exclusion principle' [21]. An example of this principle is illustrated in Fig 5E and 5F, where minor differences in division rates between phytoplankton groups (in this case, relative advantages of swimming versus sinking and vacuolation) led to a size-dependent selection for non-diatoms or diatoms. Thus, while our model sustains size diversity across all nutrient levels, it does not address the issue of species diversity within size classes. If in our combined-species model scenario the diffusion-based differences in division rate were countered by reduced grazing in small diatoms (e.g., owing to protection by frustule) and mixotrophy in larger non-diatoms, then perhaps one can imagine how a re-parameterized model could yield a sustained coexistence of both phytoplankton groups within size classes. The key point here is that 'fitness' in the plankton world is defined by any adaptation that allows persistence of a given species within a community (including beneficial and detrimental interactions between individuals), not simply acquisition of growth limiting resources. Importantly, the time-scale over which fitness is selected can be very long (years), causing shorter-term species-specific advantages to be averaged out, enabling greater sustained diversity within functional size classes [21].

Supporting information

S1 File.
(PDF)

Acknowledgments

discussions and Maurizio Ribera d'Alcalá and an anonymous reviewer for constructive comments on the manuscript.

Author Contributions

Conceptualization: Michael J. Behrenfeld.

Formal analysis: Michael J. Behrenfeld, Kelsey M. Bisson, Emmanuel Boss, Peter Gaube.

Funding acquisition: Michael J. Behrenfeld, Kelsey M. Bisson, Emmanuel Boss, Peter Gaube, Lee Karp-Boss.

Investigation: Michael J. Behrenfeld, Kelsey M. Bisson, Emmanuel Boss, Peter Gaube, Lee Karp-Boss.

Methodology: Michael J. Behrenfeld, Emmanuel Boss.

Writing – original draft: Michael J. Behrenfeld.

Writing – review & editing: Kelsey M. Bisson, Emmanuel Boss, Peter Gaube, Lee Karp-Boss.

References

1. Darwin C. The origin of species by means of natural selection. Macmillan, New York, Ed. 6, 1859

2. Hutchinson GE. The paradox of the plankton. Amer. Nat. 1961; 95: 137–145.

3. Michaelis L, Menten ML. Die kinetik der invertinwirkung. Biochem. Z 1913; 49: 333–369.

4. Poulin FJ, Franks PJ. Size-structured planktonic ecosystems: constraints, controls and assembly instructions. J. Plankt. Res. 2010; 32: 1121–1130. https://doi.org/10.1093/plankt/fbp145 PMID: 20625560

5. Taniguchi DA, Franks PJ, Poulin FJ. Planktonic biomass size spectra: an emergent property of size-dependent physiological rates, food web dynamics, and nutrient regimes. Mar. Ecol. Progr. Ser. 2014; 514: 13–33.

6. Dutkiewicz S, Cermeno P, Jahn O, Follows MJ, Hickman AE, Taniguchi DA, et al. Dimensions of marine phytoplankton diversity. Biogeosci. 2020; 17: 609–634.

7. Acevedo-Trejos E, Brandt G, Bruggeman J, Merico A. Mechanisms shaping size structure and functional diversity of phytoplankton communities in the ocean. Sci. Rep. 2015; 5: 1–8. https://doi.org/10.1038/srep08918 PMID: 25747280

8. Venrick EL. Phytoplankton in an oligotrophic ocean: species structure and interannual variability. Ecol. 1990; 71: 1547–1563.

9. Reynolds RA, Stramski D. 2021. Variability in oceanic particle size distributions and estimation of size class contributions using a non-parametric approach. J. Geophys. Res.: Oceans 2021; 126: e2021JC017946. https://doi.org/10.1029/2021JC017946 PMID: 35859706

10. Ward BA, Dutkiewicz S, Follows MJ. Modelling spatial and temporal patterns in size-structured marine plankton communities: top–down and bottom–up controls. J. Plankt. Res. 2014; 36: 1: 31–47.

11. Hulburt EM. Competition for Nutrients by Marine Phytoplankton in Oceanic, Castal, and Estuarine Regions. Ecol. 1970; 51: 475–484.

12. Siegel DA. Resource competition in a discrete environment: Why are plankton distributions paradoxical? Limnol. Oceanogr. 1998; 43: 1133–1146.

13. Partensky F, Hess WR, Vaulot D. Prochlorococcus, a marine photosynthetic prokaryote of global significance. Microbiol. Mol. Biol. Rev. 1999; 63: 106–127. https://doi.org/10.1128/MMBR.63.1.106-127.1999 PMID: 10066832

14. Martiny AC, Hagstrom GI, DeVries T, Letscher RT, Britten GL, Garcia CA, et al. Marine phytoplankton resilience may moderate oligotrophic ecosystem responses and biogeochemical feedbacks to climate change. Limnol. Oceanogr. 2022; 67: S378–S389

15. Sheldon RW, Prakash A, Sutcliffe W Hr. The size distribution of particles in the ocean 1. Limnol. Oceanogr. 1972; 17: 327–340.

16. Jonasz M, Fournier G. Light scattering by particles in water: theoretical and experimental foundations. Elsevier, 2011.

17. Huete-Ortega M, Cermeno P, Calvo-Díaz A, Maranon E. Isometric size-scaling of metabolic rate and the size abundance distribution of phytoplankton. Proc. Roy. Soc. B: Biol. Sci. 2012; 279: 1815–1823. https://doi.org/10.1098/rspb.2011.2257 PMID: 22171079

18. Marañón E. Cell size as a key determinant of phytoplankton metabolism and community structure. Ann. Rev. Mar. Sci. 2015; 7: 241–264. https://doi.org/10.1146/annurev-marine-010814-015955 PMID: 25062405

19. Behrenfeld MJ, Boss ES, Halsey KH. Phytoplankton community structuring and succession in a competition-neutral resource landscape. ISME Comm. 2021; 1: 1–8.

20. Menden-Deuer S, Lessard EJ. Carbon to volume relationships for dinoflagellates, diatoms, and other protist plankton. Limnol. Oceanogr. 2000; 45: 569–579.

21. Behrenfeld MJ, O'Malley R, Boss E, Karp-Boss L, Mundt C. Phytoplankton biodiversity and the inverted paradox. ISME Comm. 2021; 1: 1–9.

22. Tilman D, Mattson M, Langer S. Competition and nutrient kinetics along a temperature gradient: An experimental test of a mechanistic approach to niche theory 1. Limnol. Oceanogr. 1981; 26: 1020–1033.

23. Sukenik A, Bennett J, Falkowski P. Light-saturated photosynthesis—limitation by electron transport or carbon fixation? Biochim. Biophys. Acta 1987; 891: 205–215.

24. Glover HE. Ribulosebisphosphate carboxylase/oxygenase in marine organisms. Internat. Rev. Cytol. 1989; 115: 67–138.

25. Fisher T, Shurtz-Swirski R, Gepstein S, Dubinsky Z. Changes in the levels of ribulose-l, 5-bisphosphate carboxylase/oxygenase (rubisco) in *Tetraedron minimum* (chlorophyta) during light and shade adaptation. Plant Cell Phys. 1989; 30: 221–228.

26. Rivkin RB. Photoadaptation in marine phytoplankton: Variations in ribulose 1, 5-bisphosphate activity. Mar. Ecol. Progr. Ser. 1990; 62: 61–72.

27. Orellana MV, Perry MJ. An immunoprobe to measure Rubisco concentrations and maximal photosynthetic rates of individual phytoplankton cells. Limnol. Oceanogr. 1992; 37: 478–490. https://doi.org/10.4319/lo.1992.37.3.0478 PMID: 32336786

28. Flynn KJ, Raven JA. What is the limit for photoautotrophic plankton growth rates? J. Plankt. Res. 2017; 39: 13–22.

29. Jassby AD, Platt T. Mathematical formulation of the relationship between photosynthesis and light for phytoplankton. Limnol. Oceanogr. 1976; 21: 540–547.

30. Geider RJ, MacIntyre HL, Kana TM. A dynamic regulatory model of phytoplanktonic acclimation to light, nutrients, and temperature. Limnol. Oceanogr. 1998; 43: 679–694.

31. Thornley JMH. Photosynthesis In: Sutcliffe JF, Mahlberg P, editors. Mathematical models in plant physiology, 1976; pp. 11–14.

32. Laws EA, Pei S, Bienfang P, Grant S, Sunda WG. Phosphate-limited growth of *Pavlova lutheri* (Prymnesiophyceae) in continuous culture: determination of growth-rate-limiting substrate concentrations with a sensitive bioassay procedure 1. J. Phycol. 2011; 47: 1089–1097.

33. Flynn KJ, Skibinski DO, Lindemann C. Effects of growth rate, cell size, motion, and elemental stoichiometry on nutrient transport kinetics. PLoS Comput. Biol. 2018; 14: e1006118. https://doi.org/10.1371/journal.pcbi.1006118 PMID: 29702650

34. Pasciak WJ, Gavis J. Transport limitation of nutrient uptake in phytoplankton 1. Limnol. Oceanogr. 1974; 19: 881–888.

35. Shaw A, Takacs I, Pagilla K, Riffat R, DeClippeleir H, Wilson C, et al. Toward universal half-saturation coefficients: Describing extant KS as a function of diffusion. Water Environ. Res. 2015; 87: 387–391. https://doi.org/10.2175/106143015x14212658614072 PMID: 26460458

36. Armstrong RA. Nutrient uptake rate as a function of cell size and surface transporter density: A Michaelis-like approximation to the model of Pasciak and Gavis. Deep Sea Res Pt. I. 2008; 55: 1311–1317.

37. Aksnes DL, Cao FJ. Inherent and apparent traits in microbial nutrient uptake. Mar. Ecol. Progr. Ser. 2011; 440: 41–51.

38. Munk WH, Riley GA. Absorption of nutrients by aquatic plants. J. Mar. Res. 1952; 11: 215–240.

39. Jumars PA, Deming JW, Hill PS, Karp-Boss L, Yager PL, Dade WB. Physical constraints on marine osmotrophy in an optimal foraging context. Aquat. Microb. Ecol. 1993; 7: 121–159.

40. Karp-Boss L, Boss E, Jumars PA. Nutrient fluxes to planktonic osmotrophs in the presence of fluid motion. Oceanogr. Mar. Biol. 1996; 34: 71–108.

41. Berg HC. Random walks in biology. Princeton University Press, 2018.

42. Kiørboe T. A mechanistic approach to plankton ecology. Princeton University Press, 2018.

43. Laws EA. Evaluation of in situ phytoplankton growth rates: a synthesis of data from varied approaches. Ann. Rev. Mar. Sci. 2013; 5: 247–268. https://doi.org/10.1146/annurev-marine-121211-172258 PMID: 22809184

44. Brzezinski MA. Vertical distribution of ammonium in stratified oligotrophic waters. Limnol. Oceanogr. 1988; 33: 1176–1182.

45. Jones RD. An improved fluorescence method for the determination of nanomolar concentrations of ammonium in natural waters. Limnol. Oceanogr. 1991; 36: 814–819.

46. Raimbault P, Garcia N, Cerutti F. Distribution of inorganic and organic nutrients in the South Pacific Ocean− evidence for long-term accumulation of organic matter in nitrogen-depleted waters. Biogeosci. 2008; 5: 281–298.

47. Ellwood MJ, Law CS, Hall J, Woodward EMS, Strzepek R, Kuparinen J, et al. Relationships between nutrient stocks and inventories and phytoplankton physiological status along an oligotrophic meridional transect in the Tasman Sea. Deep Sea Res. Pt. I. 2013; 72: 102–120.

48. Hashihama F, Kanda J, Tauchi A, Kodama T, Saito H, Furuya K. Liquid waveguide spectrophotometric measurement of nanomolar ammonium in seawater based on the indophenol reaction with o-phenyl-phenol (OPP). Talanta 2015; 143: 374–380. https://doi.org/10.1016/j.talanta.2015.05.007 PMID: 26078173

49. Voss M, Bange HW, Dippner JW, Middelburg JJ, Montoya JP, Ward B. The marine nitrogen cycle: recent discoveries, uncertainties and the potential relevance of climate change." *Phil. Trans. Roy. Soc. B* 2013; 368: 1621, 20130121.

50. Sommer U. Some size relationships in phytoflagellate motility." In Flagellates in Freshwater Ecosystems, Springer, Dordrecht, 1988; pp. 125–131.

51. Waite A, Fisher A, Thompson PA, Harrison PJ. Sinking rate versus cell volume relationships illuminate sinking rate control mechanisms in marine diatoms. Mar. Ecol. Progr. Ser. 1997; 157: 97–108.

52. Berg HC, Purcell EM. Physics of chemoreception. Biophys. J. 1997; 20: 193–219.

53. Behrenfeld MJ, Halsey KH, Boss E, Karp-Boss L, Milligan AJ, Peers G. Thoughts on the evolution and ecological niche of diatoms. Ecol. Monogr. 2021; 91: e01457.

54. Laws EA, Bannister TT. Nutrient-and light-limited growth of *Thalassiosira fluviatilis* in continuous culture with implications for phytoplankton growth in the ocean. Limnol. Oceanogr. 2004; 49: 2316–2316.

55. Laws EA, Pei S, Bienfang P, Grant S. Phosphate-limited growth and uptake kinetics of the marine prasi-nophyte *Tetraselmis suecica* (Kylin) Butcher. Aquacult. 2011; 322: 117–121.

56. Hilborn R, Mangel M. The ecological detective. Princeton University Press, 2013.

57. Evans GT, Parslow JS. A model of annual plankton cycles. Biol. Oceanogr. 1985; 3: 327–347.

58. Moore DJ. A framework for incorporating ecology into Earth System Models is urgently needed. Glob. Chang. Biol. 2022; 28: 343–345. https://doi.org/10.1111/gcb.15915 PMID: 34619006

59. Behrenfeld MJ, Boss ES. Resurrecting the ecological underpinnings of ocean plankton blooms. Ann. Rev. Mar. Sci. 2014; 6: 167–194. https://doi.org/10.1146/annurev-marine-052913-021325 PMID: 24079309

60. Ward BA, Dutkiewicz S, Jahn O, Follows MJ. A size-structured food-web model for the global ocean. Limnol. Oceanogr. 2012; 57, 6: 1877–1891.

61. Riley GA. Factors controlling phytoplankton population on George's Bank. J. Mar. Res. 1946; 6: 54–73.

62. Behrenfeld MJ, Boss ES. Student's tutorial on bloom hypotheses in the context of phytoplankton annual cycles. Glob. Chang. Biol. 2018; 24: 55–77. https://doi.org/10.1111/gcb.13858 PMID: 28787760

63. Ibarbalz FM, Henry N, Brandão MC, Martini S, Busseni G, Byrne H, et al. Global trends in marine plankton diversity across kingdoms of life. Cell 2019; 179: 1084–1097. https://doi.org/10.1016/j.cell.2019.10.008 PMID: 31730851

64. Ward BA, Dutkiewicz S, Barton AD, Follows MJ. Biophysical aspects of resource acquisition and competition in algal mixotrophs. Amer. Nat. 2011; 178: 98–112. https://doi.org/10.1086/660284 PMID: 21670581

65. Mitchell JG, Seuront L, Doubell MJ, Losic D, Voelcker NH, Seymour J, et al. The role of diatom nano-structures in biasing diffusion to improve uptake in a patchy nutrient environment. PLoS One 2013; 8: e59548. https://doi.org/10.1371/journal.pone.0059548 PMID: 23667421

66. Caputo A, Nylander JA, Foster RA. The genetic diversity and evolution of diatom-diazotroph associations highlights traits favoring symbiont integration. FEMS Microbiol. Lett. 2019; 366: fny297. https://doi.org/10.1093/femsle/fny297 PMID: 30629176

67. Decelle J, Probert I, Bittner L, Desdevises Y, Colin V, de Vargas C, et al. An original mode of symbiosis in open ocean plankton. Proc. Nat. Acad. Sci. 2012; 109: 18000–18005. https://doi.org/10.1073/pnas.1212303109 PMID: 23071304

68. Decelle J, Stryhanyuk H, Gallet B, Veronesi G, Schmidt M, Balzano S, et al. Algal remodeling in a ubiquitous planktonic photosymbiosis. Curr. Biol. 2019; 29: 968–978. https://doi.org/10.1016/j.cub.2019.01.073 PMID: 30827917

69. Bidle KD. Programmed cell death in unicellular phytoplankton. Curr. Biol. 2016; 26: R594–R607. https://doi.org/10.1016/j.cub.2016.05.056 PMID: 27404255

70. Knowles B, Bonachela JA, Behrenfeld MJ, Bondoc KG, Cael BB, Carlson CA, et al. Temperate infection in a virus–host system previously known for virulent dynamics. Nat. Comm. 2020; 11: 1–13.

71. Brussaard CP, Riegman R. Influence of bacteria on phytoplankton cell mortality with phosphorus or nitrogen as the algal-growth-limiting nutrient. Aq. Microb. Ecol. 1998; 14: 271–280.

72. Choi CJ, Brosnahan ML, Sehein TR, Anderson DM, Erdner DL. Insights into the loss factors of phytoplankton blooms: The role of cell mortality in the decline of two inshore *Alexandrium* blooms. Limnol. Oceanogr. 2017; 62: 1742–1753.

73. Record NR, Pershing AJ, Maps F. The paradox of the "paradox of the plankton". ICES J. Mar. Sci. 2014; 71: 236–40.

74. Cropp R, Norbury J. Comment on "The paradox of the 'paradox of the plankton'" by Record et al. ICES J. Mar. Sci. 2014; 71: 293–295.

75. Behrenfeld MJ, Falkowski PG. Photosynthetic rates derived from satellite-based chlorophyll concentration. Limnol. Oceanogr. 1997; 42: 1–20.

76. Fisher NL, Halsey KH. Mechanisms that increase the growth efficiency of diatoms in low light. Photosyn. Res. 2016; 129: 183–197. https://doi.org/10.1007/s11120-016-0282-6 PMID: 27312336